Corrected: Publisher Correction

REVIEWS

Probing dynamics in quantum materials with femtosecond X-rays

*Michele Buzzi, Michael Först, Roman Mankowsky and Andrea Cavalleri**

Abstract | Optical pulses are routinely used to drive dynamic changes in the properties of solids. In quantum materials, many new phenomena have been discovered, including ultrafast transitions between electronic phases, switching of ferroic orders and non-equilibrium emergent behaviours, such as photoinduced superconductivity. Understanding the underlying non-equilibrium physics requires detailed measurements of multiple microscopic degrees of freedom at ultrafast time resolution. Femtosecond X-rays are key to this endeavour, as they can probe the dynamics of structural, electronic and magnetic degrees of freedom. Here, we review a series of representative experimental studies in which ultrashort X-ray pulses from free-electron lasers have been used, opening up new horizons for materials research.

The equilibrium functional properties of solids are determined by the interplay between many microscopic degrees of freedom. These include the crystallographic structure as well as the arrangement and dynamic fluctuations of charges, spins and orbitals. The strong interactions between these many degrees of freedom create complex energy surfaces and make the ground state highly dependent on subtle changes in the microscopic parameters and on fine-tuning of the external conditions. Understanding the origin of these emergent phenomena is, even at equilibrium, a formidable task that requires several degrees of freedom in a material to be monitored simultaneously. In the past two decades, equilibrium X-ray[1,2] and photoemission techniques[3,4] have provided an enormous amount of information and have contributed to the understanding of equilibrium emergent states.

This Review focuses on a new experimental direction in the physics of complex correlated electron systems — the use of electromagnetic fields to control emergent properties away from thermodynamic equilibrium. Indeed, ultrashort laser pulses have proved to be especially effective tools to manipulate magnetism[5,6] or ferroelectricity[7,8], to induce phase transitions at ultrafast speed[9,10] and to trigger new emergent phenomena[10–13]. The underlying physics proceeds on femtosecond and picosecond timescales. Although these timescales have been accessible since the 1970s with optical laser pulses, changes in the optical constants at visible and near-infrared frequencies provide very limited information, and this is only indirectly related to the microscopic degrees of freedom of interest.

Complementary techniques that directly interrogate charge, spin and lattice degrees of freedom in a material are therefore often used to gain deeper insight into the underlying physics. Time-resolved X-ray and electron diffraction, for example, directly track the photoinduced evolution of a crystal lattice (BOX 1), with some limitations in time resolution for electron diffraction experiments[14]. By contrast, time-resolved and angle-resolved photoemission spectroscopy (tr-ARPES) can track changes in the electronic band structure at different positions in the Brillouin zone. Similarly, knowledge of the transient element-specific local electronic structure can be gained from spectroscopic X-ray techniques, such as time-resolved X-ray absorption. Furthermore, tunable and intense X-rays provide the possibility of combining these spectroscopic techniques with the nanoscale spatial resolution of diffraction to enable the direct study of the time evolution of complex orders of charges, spins and orbitals (BOX 1). Ultimately, a comprehensive view of the underlying physics of a material can only be obtained when results from different time-resolved techniques are combined.

The development of ultrafast X-ray probes dates back at least two decades and was made possible by the development of high-intensity[15,16] amplified optical pulses[17,18]. In the 1990s, X-ray fluorescence from plasmas[19,20] spurred activity in ultrafast X-ray probe development. Despite the low flux and limited tunability of these first femtosecond X-ray sources, many rudimentary structural dynamics experiments were undertaken, including studies of laser-induced disordering of organic films[21], photoinduced melting of semiconductors[22–24], detection of coherent acoustic[25,26] and optical[27] phonons, and photoinduced solid–solid phase transitions[28]. Other techniques combined the same high-peak-power femtosecond lasers with relativistic electron beams, initially by exploiting 90° Thomson scattering[29–31] and later by using lasers as energy modulators in electron

Max Planck Institute for the Structure and Dynamics of Matter, Hamburg, Germany.

**e-mail: andrea.cavalleri@mpsd.mpg.de*

https://doi.org/10.1038/s41578-018-0024-9

storage rings[32–35]. The photon energies of these storage-ring-based sources are tunable and opened the door to femtosecond X-ray spectroscopies, such as ultrafast near-edge X-ray absorption spectroscopy[36] and X-ray magnetic circular dichroism[37]. Accelerator-based sources brought about multiple-order-of-magnitude improvements in the X-ray flux[38,39] and culminated in the demonstration of X-rays from the operation of a free-electron laser (FEL)[40].

In this Review, we discuss the evolution of ultrafast materials research that has followed the introduction of X-ray FELs, focusing on how ultrafast X-ray diffraction and spectroscopy have been used to investigate ultrafast processes in quantum materials. We highlight representative experiments, with a focus on studies that involve the ultrafast rearrangement of ferroic orders or of coupled charge, spin and orbital dynamics in complex oxides and other strongly correlated materials. The notable case of photoinduced superconductivity is also discussed, especially with respect to the contributions made by X-ray FEL experiments.

Box 1 | **Time-resolved X-ray techniques**

Pump–probe X-ray techniques are a valuable tool for reconstructing materials dynamics, as they can directly capture transient light-induced changes in microscopic degrees of freedom. In a typical X-ray time-resolved experiment (see the figure), the sample under study is excited with a strong laser pulse, termed the pump pulse, which triggers a dynamic response in the material. A time-delayed X-ray pulse probes the pump-induced changes through interaction with the material, and the scattered (or transmitted) beam is subsequently collected by a detector. Depending on the choice of photon energy in the hard and soft X-ray regimes, information about the atomic or electronic structure of the material can be obtained using techniques such as X-ray diffraction, X-ray absorption spectroscopy and resonant X-ray diffraction.

Discovered by Max von Laue in 1912, X-ray diffraction is arguably one of the most useful tools for materials characterization. X-ray waves are scattered by the periodically ordered atoms in a crystal and interfere either constructively or destructively along specific directions. Analysis of the measured interference patterns enables the average position of each atom in the crystal to be determined with sub-picometre spatial resolution. For example, by monitoring the position and relative intensities of a chosen set of Bragg peaks as a function of time, the lattice dynamics triggered by the excitation of a coherent phonon can be traced[25–27]. With the symmetry of the material determining the measured diffraction pattern, the stages through which an ultrafast light-induced phase transition occurs can be followed[28]. Moreover, in analogy to the case of thermal diffuse scattering, the time dependence of the scattered intensity in between Bragg peaks reveals information about the dispersion of phonons without the need for ab initio modelling of force constants[148].

X-ray absorption spectra contain fingerprints of the electronic and magnetic structures of materials. The X-ray energy is tuned to be in resonance with an atomic transition, which substantially increases the absorption, enabling the electronic and magnetic states to be reconstructed in an element-specific manner. By analysing how the absorption spectrum of a substance changes upon photoexcitation, it is possible, for example, to gain insight into transient changes in the oxidation states and bond lengths of a compound[127,158]. In addition, changes in the magnetic moment of a specific atom can be determined by measuring the X-ray magnetic circular dichroism spectrum under resonance conditions[159].

Absorption spectroscopy captures sample properties without the possibility of spatial reconstruction, making it difficult to observe complex long-range ordering of charges, spins and orbitals. Resonant X-ray diffraction, however, combines the contrast mechanisms of absorption spectroscopy with the spatial resolution of diffraction. By performing diffraction experiments with incoming photons tuned to be in resonance with appropriate atomic transitions, it is possible to directly study phenomena such as charge stripe order in cuprates[131,132] or orbital and spin order in manganites[78,80]. In recent years, this technique has been developed to operate in the time domain and has become a standard experiment for materials research at X-ray free-electron laser facilities.

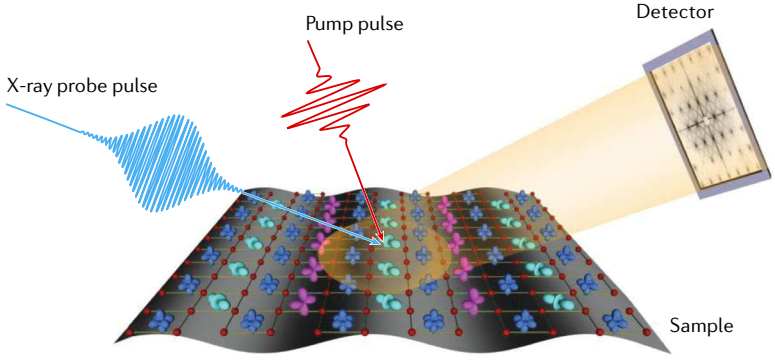

Ferroic materials

Ultrafast ferroelectric switching. Ferroelectric materials are of great scientific and technological interest, as they exhibit bistable, structurally distorted states of oppositely phased electrical polarization. Owing to these properties, digital information can be stored in ferroelectrics, making them interesting candidates for non-volatile memory devices. Typically, switching of the ferroelectric polarization is achieved by the application of pulsed electric fields. However, this ferroelectric switching is driven by incoherent dynamics and the propagation of domain boundaries, which limit switching times to hundreds of picoseconds[41–43]. Several attempts to achieve ultrafast ferroelectric switching have been made by driving the ferroelectric soft mode coherently with light pulses, either with impulsive Raman scattering[34,44–46] or direct excitation[8,47].

The properties of ferroelectrics can be controlled, for example, by the photoexcitation of charge carriers across the bandgap or by the excitation of impurity levels. Such approaches have been used to facilitate polarization switching, control the domain nucleation and induce self-organized domain patterns[48–51]. The structural dynamics of $PbTiO_3$ thin films in the ferroelectric phase were shown to involve a distortion of the unit cell along the *c* axis upon photoexcitation with short ultraviolet pulses[52]. The response of the lattice constant along this direction was extracted from changes in the time-resolved X-ray scattering angle of an out-of-plane diffraction peak. A fast contraction of the film within the first 5 ps is followed by a long-lived expansion of the lattice. This expansion is driven by dynamic charge screening of the depolarization field, which in thin-film ferroelectrics acts against the ferroelectric polarization[53].

The structural response of $Sn_2P_2S_6$ in its ferroelectric phase to the direct excitation of its soft mode was also measured with X-ray probes[54]. Following excitation with terahertz pulses with a 120 kV cm^{-1} peak electric field, coherent oscillations of the atoms along the soft-mode coordinate were measured through the corresponding modulation of the intensity of selected Bragg peaks. The amplitude of these motions corresponded to a change of only 8% in the ferroelectric polarization. It was extrapolated that switching may become possible if the terahertz electric field were to be increased to 1 MV cm^{-1}.

In this context, the development of mode-selective lattice control, so-called nonlinear phononics, has

opened up new opportunities in ferroelectrics[55]. Transient reversal of the ferroelectric polarization[7] was observed using nonlinear optical probes, an important achievement that will likely motivate structural studies of the involved atomic motions using ultrafast X-ray scattering.

Ultrafast magnetism. Although it has long been known that light can be used to destabilize ferromagnetism through inverse magneto-optical effects[56–58], it has more recently been shown that ultrashort optical pulses can perturb magnetism along a highly non-equilibrium path and hence far faster than expected[6,59–61]. Time-resolved X-ray absorption spectroscopy and X-ray magnetic circular dichroism have been used to provide new insight into this class of processes, rejuvenating the field. For example, these two techniques were combined to reconstruct the dynamic response in a Ni thin film excited with short near-infrared pulses[37]. Within ~100 fs after optical excitation, the ferromagnetic order was completely quenched, indicating ultrafast transfer of spin angular momentum to auxiliary degrees of freedom, presumably the crystal lattice.

Resonant X-ray scattering measurements with simultaneous spatial resolution have been used to study the growth of the magnetic disorder in magnetic thin films, evidencing the role of photoexcited electron diffusion on a length scale of only tens of nanometres[62]. For example, single soft X-ray pulses from a FEL were used to record diffraction patterns from nanoscale magnetic-domain structures[63]. This approach yielded magnetic correlations with nanometre precision and a time resolution of 30 fs. Moreover, magnetic small-angle X-ray scattering was used to analyse modifications of the magnetic-domain structure in a Co/Pd multilayer sample induced by near-infrared laser pulses[64]. These measurements revealed that the quenching of the spin angular momentum is accompanied by a decrease in the magnetic spatial correlations within the first few hundred femtoseconds. From its very high speed, it was speculated that this change in magnetic spatial correlation could not result from domain wall motion but was rather caused by spin-dependent transport of photoexcited electrons between neighbouring ferromagnetic domains.

Magnetic X-ray scattering experiments have also had a key role in determining the importance of nanoscale inhomogeneities on ultrafast magnetization switching in GdFeCo, a collinear ferrimagnet with a strong magneto-optical response[65]. Near-infrared laser pulses were used to excite electrons on a timescale shorter than that of exchange interactions (~100 fs), reversing the total magnetization of this compound after each pulse[6,66,67]. Small-angle X-ray scattering was used to gain insight into the mechanisms that may be responsible for this ultrafast switching[5]. The chemical inhomogeneities in GdFeCo occur on a 10 nm length scale and divide the material into Gd-rich and Fe-rich regions (FIG. 1a). From the magnetic diffraction signal, S_q, at low scattering momenta ($q < 0.2\,nm^{-1}$), it is possible to retrieve the average sample magnetization of the Gd and Fe spin sublattices, which are oppositely aligned at equilibrium. The net magnetizations of both the Gd and Fe spin sublattices are quenched rapidly within 1 ps after excitation (FIG. 1b, top part). The S_q at high scattering momenta ($q > 0.2\,nm^{-1}$), however, is sensitive to the nanoscale structure of GdFeCo and showed significantly different dynamics (FIG. 1b, bottom part). Within the first picosecond, the signal from the Fe 3*d* spins substantially decreased, whereas the signal from the Gd 4*f* spins increased dramatically, which was interpreted as non-local transfer of angular momentum from the Fe-rich to the Gd-rich regions (FIG. 1c). Although magnetic switching was not directly observed, angular momentum transfer is probably relevant to the understanding of ultrafast magnetization reversal.

In addition to ferromagnetic and ferrimagnetic metallic compounds, time-resolved X-ray scattering techniques are also powerful tools for clarifying the ultrafast dynamics in materials with antiferromagnetic ordering. Over the past 10 years, resonant X-ray scattering[2,68,69] has been extended to the time domain and has emerged as a powerful technique to follow ultrafast dynamics with element specificity and with sensitivity on nanometre length scales. The first reported femtosecond resonant X-ray scattering experiment was performed on the magnetic semiconductor EuTe at the Eu M-edge and demonstrated that the optical excitation of the $4f \rightarrow 5d$ transition reduces antiferromagnetic order on the Eu sites with a time constant of <700 fs (REF.[70]). It was speculated that exchange interactions were modified as a result of optically induced lattice deformations that occur on the timescale of acoustic motion.

More recently, time-resolved resonant X-ray scattering has been used to probe magnetization dynamics in antiferromagnetic Ho (REF.[71]). On each Ho atom, the total magnetic moment is carried mostly by the localized 4*f* electrons and only partially by the itinerant 5*d* electrons that form the valence band. Time-resolved resonant magnetic scattering at different atomic transitions was used to separately reconstruct the dynamics of the localized 4*f* and 5*d* spins when near-infrared femtosecond pulses selectively excited the 5*d* electrons. The experiment showed that the 4*f*–5*d* exchange coupling is so strong that the spins on these different electrons were quenched on the same timescale.

Lastly, magnetic scattering allows for imaging of magnetization dynamics using X-ray holography[72]. In 2012, the possibility of collecting high-quality magnetic holograms using femtosecond soft X-ray pulses was first demonstrated[73]. More recently, the same technique was used to directly image ultrafast demagnetization dynamics at domain wall boundaries in a Co/Pd compound[74], confirming previous observations[64]. Moreover, combined X-ray photon correlation spectroscopy with coherent resonant magnetic X-ray scattering has been used to study spontaneous fluctuations of magnetic skyrmions on nanosecond timescales[75]. These results illustrate that X-ray photon correlation spectroscopy can now be used to study excitations in the μeV energy range, making it complementary to inelastic X-ray and neutron scattering, which are typically limited to the study of excitations in the meV energy range.

The area of femtosecond magnetism has made extensive use of ultrafast X-ray sources. In addition, these experiments have been effective in developing a

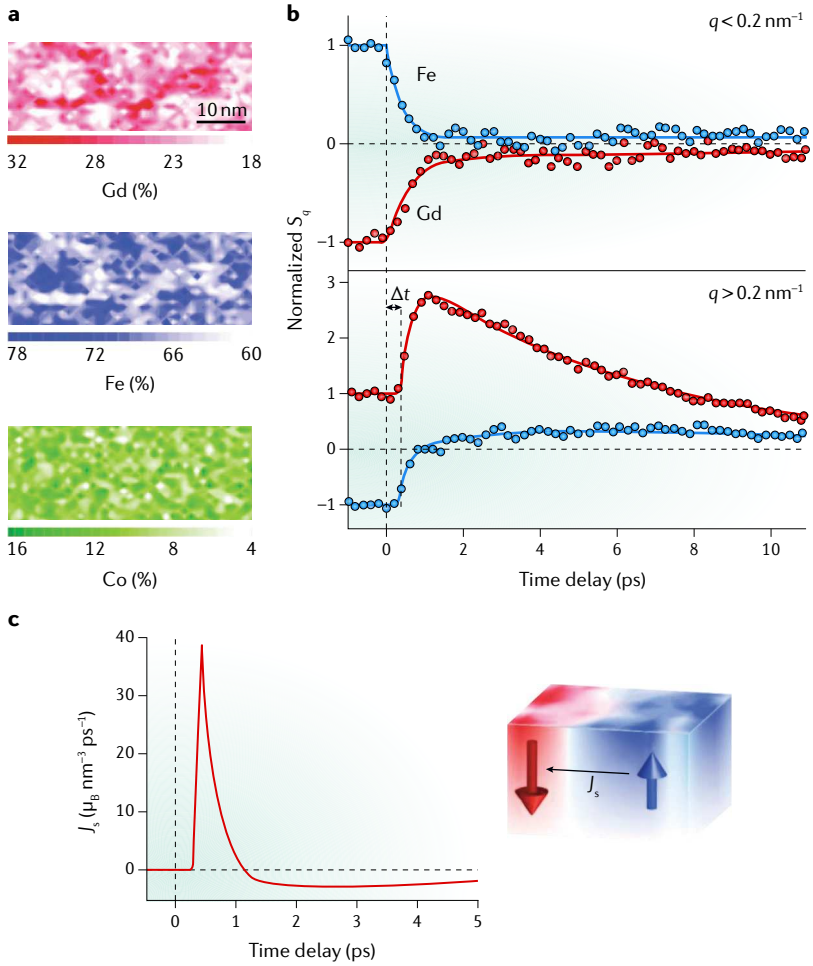

Fig. 1 | **Ultrafast angular momentum transfer in a ferromagnetic film.** Non-local, ultrafast transfer of angular momentum in GdFeCo was revealed by time-resolved magnetic small-angle X-ray scattering[5]. **a** | Local chemical nanoscale variations for Gd, Fe and Co in $Gd_{24}Fe_{66.5}Co_{9.5}$ as measured with energy-dispersive X-ray spectroscopy. Darker coloured areas indicate elemental enrichment, whereas white areas indicate below average concentrations. **b** | Temporal evolution of the magnetic diffraction, S_q, for Gd 4*f* (red) and Fe 3*d* (blue) spins. The measurement of S_q at low scattering momenta (q) (top part) probes the average sample magnetization, whereas the high-q S_q (bottom part) measures the evolution of the magnetization at the nanoscale, showing the transfer of angular momentum to the Gd-rich regions. The delay (Δt) observed for high scattering momenta indicates that the non-local angular momentum transfer occurs effectively only after ~360 fs. **c** | Time evolution of the angular momentum transfer (J_s) to the Gd-rich regions as extracted from the analysis of the high-q S_q scattering data. The ultrafast transfer of angular momentum takes 1 ps and is followed by a slow recovery through spin dissipation within the Gd regions. Adapted from REF.[5], Macmillan Publishers Limited.

whole set of new techniques, which will have an increasing impact on this and other areas of non-equilibrium dynamics as FEL sources grow in number and improve in the stability of the delivered pulses, for example, with respect to intensity, photon energy and bandwidth.

Complex oxides

Intertwined dynamics in oxides. Many transition metal oxides with fractionally filled *d* shells exhibit interesting collective phenomena that are attributable to strong electronic correlations. In particular, new phases emerge that are not captured by the familiar concepts of band theory and classical magnetism. These phases are also delicate, in that they can be easily switched by external stimulation, for example, with either static magnetic or electric fields or hydrostatic pressure. Excitation with light can also tip the balance between stable phases, sometimes switching the electronic properties on ultrafast timescales. As discussed above, femtosecond resonant soft X-ray scattering (RSXS) is a natural tool to study the evolution of these electronic or magnetic degrees of freedom. In combination with time-resolved hard X-ray scattering, which is used to track atomic structural rearrangements, or terahertz spectroscopy, which measures the optical conductivity, time-resolved RSXS directly determines how the electronic ordering is affected and through which stages the phase transition occurs.

For example, in photo-irradiated magnetite (Fe_3O_4)[76,77], time-resolved Fe L_3-edge RSXS was used to track the evolution of the electronic order after excitation. At equilibrium, the low-temperature charge-ordered phase of magnetite can be described as a network of lattice distortions encompassing three Fe sites with different valence: two Fe^{3+} sites and one Fe^{2+} site. These three-Fe-site distortions are termed trimerons[77]. The dynamic changes observed in the time-resolved measurements were interpreted in terms of the breaking of Fe trimerons followed by the creation of mobile charges[9].

Resonant diffraction can also be applied at metal K-edges to measure charge and orbital order on the metal sites in complex oxide compounds[78,79]. When combined with non-resonant scattering, this technique can be used to measure the dynamic interplay between charges and the lattice, as demonstrated in the case of the optically induced insulator–metal transition in the manganite $Pr_{0.5}Ca_{0.5}MnO_3$ (REF.[80]). In this material, the equilibrium charge order is connected to long-range orbital order and to a Jahn–Teller distortion of the crystal lattice[81]. Time-resolved X-ray scattering techniques were used to track the time evolution of these orders. Both near-infrared optical excitation[80] and resonant excitation of the Mn–O stretching vibrations[82] were shown to melt the charge order, which was followed by relaxation of the Jahn–Teller distortion and the orbital order.

Time-resolved RSXS experiments were performed on single-layer manganite $La_{0.5}Sr_{1.5}MnO_4$, in which charges, orbitals and spins form the so-called CE-type ordering pattern[83]. Near-infrared excitation of the charge carriers perturbed short-range spin ordering very effectively[84], whereas the long-range Jahn–Teller distortions and resulting orbital order were only weakly affected[85].

Mid-infrared resonant driving of a Mn–O lattice mode was also shown to perturb spin, charge and orbital order in $La_{0.5}Sr_{1.5}MnO_4$ (REF.[86]). This result was interpreted in the context of nonlinear lattice dynamics[87–89]: the crystal lattice is displaced along the coordinates of an anharmonically coupled Jahn–Teller mode to exert a force on the spin and orbital order. Similar experiments were performed on the layered nickelate $La_{1.75}Sr_{0.25}NiO_4$ (REFS[90,91]), in which charges and spins order in stripes within the Ni–O planes. Time-resolved RSXS studies at the Ni L-edge revealed that near-infrared electronic[92,93], as well as mid-infrared lattice[94], excitations also melt the charge and spin order in $La_{1.75}Sr_{0.25}NiO_4$.

In multiferroic materials, (anti)ferromagnetic order and ferroelectricity coexist and interact through magnetoelectric coupling[95–97]. Intense terahertz electric field pulses were used to resonantly drive an electromagnon and coherently control the spin order in multiferroic $TbMnO_3$ (REF.[98]). Time-resolved RSXS was subsequently used to demonstrate that the multiferroic order can be controlled on the sub-picosecond timescale; this observation could provide new opportunities for high-speed optical data storage devices.

Short-pulse optical excitations have also been used to tip the balance between different magnetically ordered states[99]. CuO exhibits lattice-commensurate (CM) collinear antiferromagnetic order in the ground state but non-collinear incommensurate (ICM) antiferromagnetism in a multiferroic state at intermediate temperatures of around 220 K (REF.[100]). Although the two phases typically coexist in different domains, near-infrared excitation induced a partial change of the average magnetic order in favour of the ICM state. Strikingly, rather than starting immediately after photoexcitation, the phase transition begins after a certain delay that depends on the intensity of the photoexcitation. It was speculated that the magnetic phase transition might be mediated by acoustic-branch magnetic excitations in analogy to the way that structural phase transitions are mediated by phonons. As the energy barrier between the ICM and CM phase decreases with increasing excitation energy, the time delay approaches the lower limit of 400 fs, equivalent to one-quarter of the oscillation period of a spin wave in this material.

Recently, time-resolved RSXS was used to study the spin-scattering dynamics in the skyrmion and conical phases of Cu_2OSeO_3 upon excitation with near-infrared and ultraviolet pulses[101]. This material has a complex phase diagram with many competing phases that exhibit different magnetic structures[102], and the application of an external magnetic field to the conical phase creates a skyrmion phase. Skyrmions are topologically protected spin configurations that have recently attracted attention for their robustness to external perturbations and for their potential in data storage applications[103]. Interestingly, the time-resolved study on Cu_2OSeO_3 showed that the skyrmion phase is more robust to optical excitation than the conical phase, possibly because different spin-scattering processes are involved in the two phases.

Oxide heterostructures. Complex oxide heterostructures have attracted significant interest over the past few years, as interfacial coupling enables the static electronic and magnetic material properties to be manipulated and new functionalities, such as superconductivity, magnetism or ferroelectricity, to be created at equilibrium[104]. The interfacial coupling was extended to ultrafast timescales when mid-infrared light fields, made resonant with specific phonon modes of the substrate, were used to trigger interfacial distortions and to dynamically modify the electronic properties of functional films. This was vividly demonstrated for a $LaAlO_3/NdNiO_3$ heterostructure[105]: large-amplitude excitation of the Al–O stretching mode in the $LaAlO_3$ substrate induced an ultrafast insulator–metal transition in the $NdNiO_3$ thin film[105]. Detailed insight into the spatiotemporal evolution of the different degrees of freedom of this ultrafast strain engineering phenomenon was obtained through a set of resonant and off-resonant X-ray diffraction experiments in which the concomitant dynamics of antiferromagnetic order[106], charge disproportionation and lattice dynamics[107] in the $NdNiO_3$ film were investigated. Time-resolved RSXS at the 852 eV Ni L_3-edge was used to measure the dynamic change in the (¼ ¼ ¼) diffraction peak of the $NdNiO_3$ thin film (FIG. 2a). The observed reduction in the peak intensity and concomitant broadening indicate heterogeneous melting of the antiferromagnetic order. The time evolution of the intensity of the (2½ 2½ 2½) peak was measured both on-resonance and off-resonance with the 8.34 keV Ni K-edge (FIG. 2b). The on-resonance intensity includes a charge order contribution (grey shaded region, FIG. 2b) that disappears on a timescale shorter than that of the off-resonance intensity, which is sensitive only to structural dynamics. Combining these different measurements enables the $NdNiO_3$ lattice, magnetic and insulator–metal dynamics to be extracted (FIG. 2c). The different types of order–disorder fronts were found to propagate from the interface into the nickelate film at different speeds (FIG. 2c,d), with melting of the charge order advancing supersonically ahead of demagnetization and structural relaxation, presumably setting the speed for the insulator–metal transition.

Charge density wave materials. Charge density waves (CDWs) are periodic modulations of the valence electron density in materials. CDWs emerge in materials with strong electron–phonon coupling, for which the total electron energy is reduced by a periodic modulation of the crystal lattice, resulting in either a static (pinned to the lattice) or dynamic (sliding) pattern at sufficiently low temperatures. As a result of the periodic modulation, a small energy gap forms at the Fermi energy at the wave vector, q, of the periodic modulation. CDWs exhibit peculiar electrical properties, such as nonlinear currents in response to alternating and direct current electric fields, which have attracted significant interest for electronic device technologies over the past several decades[108,109].

When driven out of equilibrium, the structural and electronic degrees of freedom, which are intertwined at equilibrium, may decouple and respond differently on ultrafast timescales[110–114]. Among the most studied cases of photoinduced dynamics in CDW materials is $K_{0.3}MoO_3$ (blue bronze), which exhibits a 1D CDW along otherwise metallic chains of corner-sharing MoO_6 octahedra. Time-resolved experiments showed that above a certain light intensity threshold, the excitation of blue bronze with ultrashort infrared and visible pulses melts the CDW order on femtosecond timescales[115–118]. Complementary studies using ultrafast X-ray scattering revealed that coherent oscillations of the CDW amplitude mode are triggered by a rapid reshaping of the lattice potential that causes a structural relaxation within 100 fs (REF.[119]). Indications of a more complex interplay between structural and electronic degrees of freedom

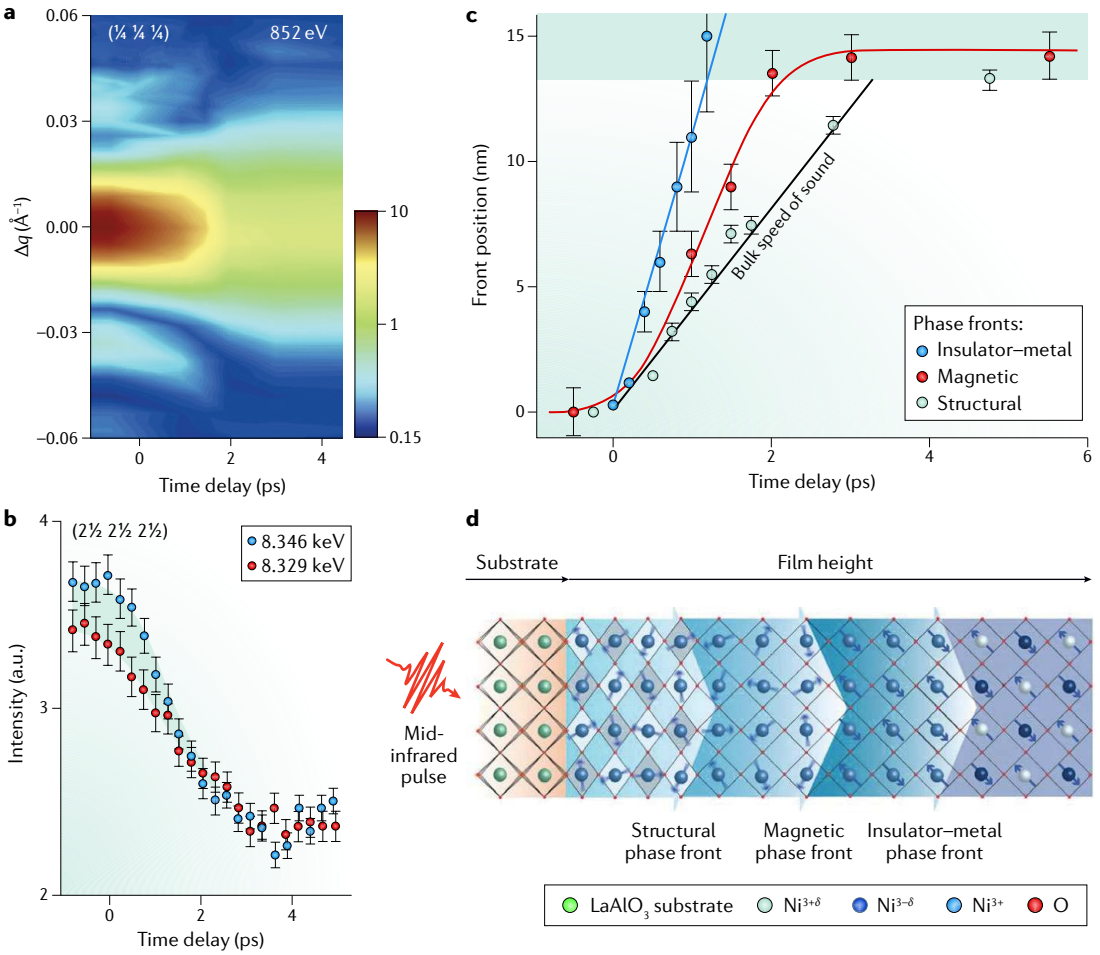

Fig. 2 | **Ultrafast interfacial strain engineering.** In a $LaAlO_3$/$NdNiO_3$ heterostructure, the dynamics of multiple magnetic, electronic and structural degrees of freedom in the $NdNiO_3$ thin film can be observed when an insulator–metal transition is driven by resonant excitation of a high-frequency vibrational mode in the underlying $LaAlO_3$ substrate. **a** | Transient momentum-resolved intensity of the (¼ ¼ ¼) diffraction peak measured at the 852 eV Ni L_3-edge, which is sensitive to antiferromagnetic ordering. The diffraction intensity is colour-coded on a logarithmic scale. **b** | Transient peak intensity of the $NdNiO_3$ (2½ 2½ 2½) reflection measured at X-ray energies resonant (8.346 keV, blue) and off-resonant (8.329 keV, red) with the Ni K-edge. The measured resonant diffraction intensity includes a charge order contribution (grey shaded region), which disappears on a timescale shorter than that of the off-resonant intensity, sensitive only to structural dynamics. **c** | Spatiotemporal evolution of the $NdNiO_3$ lattice, magnetic and insulator–metal dynamics along the out-of-plane direction of the thin film, extracted from the time-resolved diffraction experiments. Individual phase fronts of insulator–metal, antiferromagnetic–paramagnetic and structural transitions propagate at different speeds from the $LaAlO_3$/$NdNiO_3$ heterointerface into the nickelate film. **d** | Illustration of these dynamics induced by the substrate phonon excitation. Panel **a** is adapted from REF.[106], Macmillan Publishers Limited. Panels **b–d** are adapted with permission from REF.[107], American Physical Society.

were also found when the response of the CDW order was compared with optical excitation of either the electronic subsystem or the crystal lattice with mid-infrared pulses[120]. For both types of excitation, the onset of melting was found above the same threshold magnitude of the coherently driven amplitude mode oscillations, highlighting the existence of a universal stability limit for CDWs, reminiscent of the Lindemann criterion for the melting of a crystal lattice. In view of the interplay with other types of orders, most prominently Cooper pairing in high-temperature superconductors, and given their role in the formation of emergent functionalities, the study of CDWs remains a key area of research in ultrafast condensed-matter science.

Superconductors

Light-induced superconductivity in cuprates. Hole-doped cuprates of the type $YBa_2Cu_3O_{6+x}$ are a family of high-temperature superconductors that crystallize in a perovskite structure characterized by CuO_2 bilayers that stack along the *c* axis and alternate with thicker layers containing Ba, Cu and O atoms (FIG. 3a). Coherent tunnelling of Cooper pairs between adjacent CuO_2 bilayers along the crystal *c* axis results in 3D coherent transport below the critical temperature. Superconductivity is strongly enhanced by a reduction of the distance, *d*, between apical O and planar Cu atoms, which can be achieved at equilibrium by the application of pressure in the range of a few kilobars[121–124]. This relation between

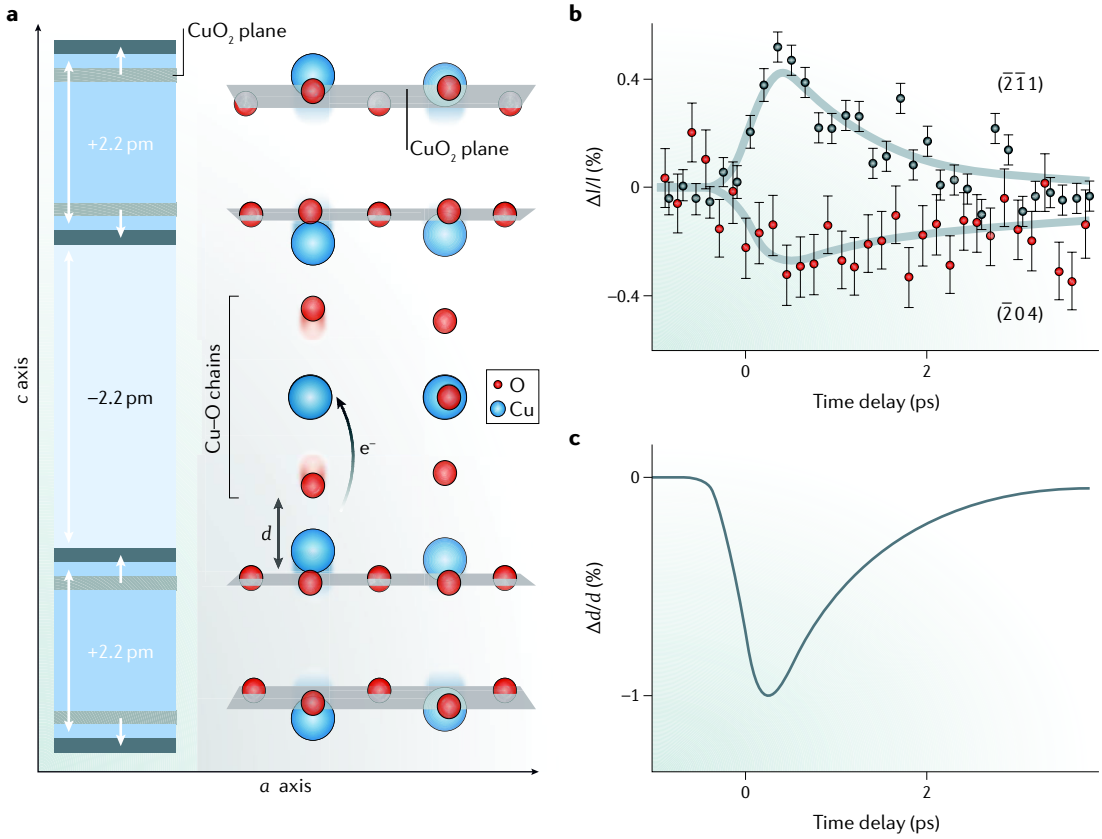

Fig. 3 | **Nonlinear phononics in a bilayer cuprate.** Signatures of nonlinear phonon coupling in the high-temperature superconductor $YBa_2Cu_3O_{6.5}$ can be identified upon driving the B_{1u} phonon mode to large amplitudes with 15 µm ultrashort laser pulses. **a** | Schematic illustration of the crystal structure of bilayer $YBa_2Cu_3O_{6.5}$ (right). CuO_2 bilayers (grey) are oriented perpendicular to the *c* axis and alternate with thicker layers containing Ba, Cu and O atoms. Y and Ba atoms are not shown for clarity. *d* is the distance between an apical O atom and a Cu atom in the plane. Nonlinear coupling of the driven B_{1u} mode to A_g modes induces changes in the intra-bilayer (+2.2 pm) and inter-bilayer (−2.2 pm) distances (left). Light and dark grey represent the CuO_2 planes in the equilibrium and driven positions, respectively. **b** | Transient intensity, *I*, of two exemplary Bragg peaks. The solid curves are obtained from the ab initio calculated structure by considering nonlinear phonon coupling of the driven B_{1u} mode to the A_g modes. **c** | Time-resolved change in the O–Cu distance *d* obtained from the calculated structure. Adapted from REF.[126], Macmillan Publishers Limited.

the superconducting properties and lattice distortions opens up interesting opportunities for the control of superconductivity with light. Mid-infrared pulses were used to resonantly excite large-amplitude oscillations in *d*, which induced picosecond-lived signatures of coherent transport above the critical temperature and even up to room temperature[12,125]. The underlying dynamics of the crystal lattice were clarified in time-resolved X-ray diffraction experiments[126]. Light-induced changes in the intensity of selected Bragg reflections that are sensitive to the motion of Cu and O ions along the *c* axis were measured to identify transient atomic rearrangements locked to the appearance and decay of the transient superconducting state (FIG. 3b). In the framework of nonlinear lattice dynamics[87], anharmonic coupling of the resonantly driven Cu–O stretching mode to Raman-active lattice modes was expected to displace the crystal lattice quasi-statically along the coordinates of the latter.

A key component of the photoinduced motions in $YBa_2Cu_3O_{6.5}$ at 100 K is the transient reduction in the important apical O to planar Cu distance (FIG. 3c). In analogy with static pressure-induced effects, this motion may facilitate light-induced coherent Cooper-pair transport along the crystal *c* axis above the equilibrium critical temperature (T_C = 50 K), as identified by density functional theory (DFT) calculations of the electronic structure in the transient state[126]. Among other effects, the DFT calculations predicted the transfer of electrons from the CuO_2 planes to the Cu–O chains, similar to what is observed upon static hole doping. This interpretation was supported by femtosecond resonant soft X-ray absorption experiments[127].

In high-temperature cuprate superconductors with doping levels close to 12.5%, superconductivity competes with the ordering of charges to reduce the critical temperature. The best-known examples are 2D CDWs in bilayer $YBa_2Cu_3O_{6+x}$ for $x \approx 0.6$ (REFS[128,129]) and charge stripes in single-layer $La_{2-x}Ba_xCuO_4$ compounds for $x = 0.125$ (REFS[130,131]) (FIG. 4a). To understand light-induced superconductivity, it is important to establish how these competing orders evolve when the transient superconducting states are formed from the charge-ordered state.

Time-resolved RSXS at the O K-edge was used to observe the rapid and complete melting of the stripe

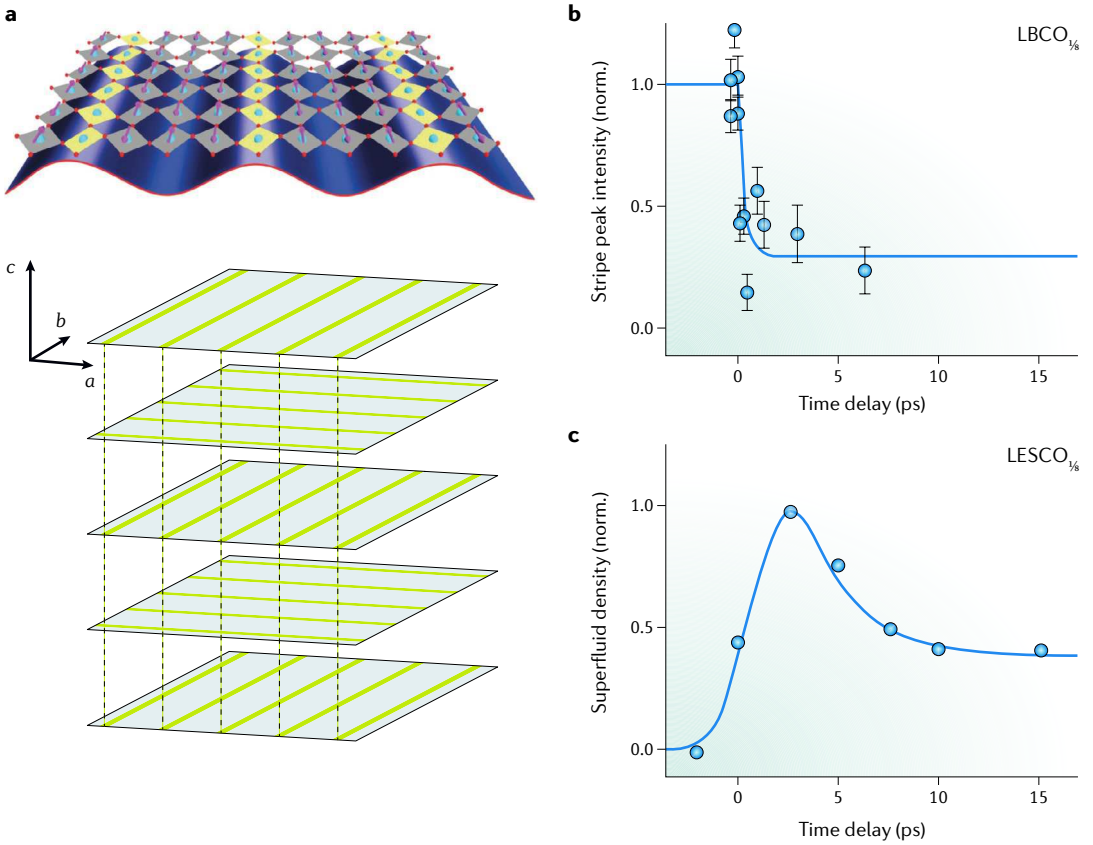

Fig. 4 | **Ultrafast stripe order melting in a single-layer cuprate.** Stripe order melting in the single-layered high-temperature superconductor $La_{1.875}Ba_{0.125}CuO_4$ ($LBCO_{1/8}$) can be triggered by driving an in-plane Cu–O stretching mode to large amplitudes with 14.5 μm ultrashort laser pulses. **a** | Illustration of the in-plane stripe order in single-layered cuprates and the 1D modulation of charges and spins responsible for suppressing superconductivity at equilibrium (top), emphasizing buckling in the Cu–O planes (Cu atoms are blue, O atoms are red and the spins are represented by arrows). The stripes are periodically stacked along the *c* axis with a 90° rotation between adjacent layers (bottom). **b** | Transient intensity of the stripe order diffraction peak at the (0.24 0 0.5) wave vector, measured in $LBCO_{1/8}$ at resonance with the O K-edge at 528 eV. **c** | Evolution of the normalized (norm.) superfluid density in $La_{1.675}Eu_{0.2}Sr_{0.125}CuO_4$ ($LESCO_{1/8}$), a compound closely related to $LBCO_{1/8}$, in which excitation of the same Cu–O stretching mode induces a transient superconducting state. Panels **a** and **b** are adapted with permission from REF.[132], American Physical Society. Panel **c** is adapted with permission from REF.[11], AAAS.

order in the frustrated superconductor $La_{1.875}Ba_{0.125}CuO_4$ following illumination by intense mid-infrared pulses resonant with the in-plane Cu–O stretching mode[132]. Superconductivity is also quenched by charge ordering in the closely related compound $La_{1.675}Eu_{0.2}Sr_{0.125}CuO_4$. In this material, the same mid-infrared excitation induces transient superconductivity, which was probed by time-resolved terahertz spectroscopy[11]. The combination of results from these two experiments (FIG. 4b,c) strongly suggests that melting of the competing stripe order is a prerequisite for the formation of the transient superconducting state. A similar result was found in $La_{1.885}Ba_{0.115}CuO_4$, in which, at certain temperatures, superconductivity and stripe order coexist at equilibrium[131]. The photoinduced destruction of charge order in $La_{1.885}Ba_{0.115}CuO_4$, measured by time-resolved RSXS, appears to be concomitant with the dynamic enhancement of the superconducting order observed in time-domain terahertz spectroscopy[133].

This dynamic interplay of competing orders was also observed in $YBa_2Cu_3O_{6.6}$ above the equilibrium critical temperature. The resonant optical excitation of the apical O vibrational mode, which, as discussed above, induces out-of-plane interlayer coherence, partially melts the in-plane CDW order, as identified in a time-resolved RSXS experiment at the 932 eV Cu L_3-edge[134].

For the first time, X-ray scattering measurements, as reported in these studies, were successfully able to capture the crystallographic and electronic properties of transient room-temperature superconductors. These findings may lead to the identification of new pathways towards the design of novel materials exhibiting equilibrium room-temperature superconductivity.

Electron–phonon coupling in high-temperature superconductors. As demonstrated in many of the above cases, combining direct measurements of the lattice structure with measurements of the electronic degree of freedom provides new insights into the emergence of exotic states of matter. Information from complementary experiments, such as time-resolved X-ray diffraction and tr-ARPES, can clarify the strength and origin of electron–phonon coupling in complex materials. For example, upon photoexcitation, global oscillations

of the Fermi level were observed using tr-ARPES in $BaFe_2As_2$, a parent compound of FeAs-based high-temperature superconductors. The frequency of these oscillations coincided with that of the A_{1g} phonon mode, suggesting the presence of a strong electron–phonon coupling[135]. These results were complemented by ultrafast X-ray diffraction experiments[136,137] that quantified how the coherent excitation of the A_{1g} mode modulates the Fe–As–Fe bond angle. In combination, these measurements lead to an estimate of the electron–phonon deformation potential and coupling constant for the A_{1g} mode, which was in good agreement with the DFT-calculated value.

More recently, it has been proposed that electronic correlations strengthen electron–phonon coupling in iron selenide (FeSe) and iron pnictide superconductors and may have a role in the emergence of superconductivity in these materials[138]. In a pioneering experiment, the electron–phonon coupling in FeSe superconductors was quantified[139]. Photoexcitation of FeSe with 1.5 eV femtosecond pulses triggered a coherent oscillation of the A_{1g} mode. Time-resolved hard X-ray diffraction tracked the displacement of the Se atom, δZ_{Se} (FIG. 5a), while high-resolution tr-ARPES tracked the shift of the $d_{XZ/YZ}$ and d_{Z^2} orbital bands (FIG. 5b,c, respectively). These measurements yielded orbital-resolved values for the electron–phonon deformation potential that could be compared directly with predictions from theory. The experimental values could be reproduced only when DFT was combined with dynamical mean-field theory to include electron–electron correlation effects, indicating their importance in determining electron–phonon coupling in FeSe and related materials.

New frontiers

Time-resolved resonant inelastic X-ray scattering. Probing low-energy excitations in solids and their dispersion reveals information about the fundamental interactions. Resonant inelastic X-ray scattering (RIXS) is a photon-in photon-out technique that can be used to study elementary excitations in solids at finite momenta with orbital and element selectivity[140]. Several elementary excitations can be probed using RIXS, including charge-transfer excitations and *d*–*d* transistions[141,142], magnons in two or three dimensions[143,144] and phonons[145,146]. Time-resolved RIXS enables reconstruction of the time evolution of such excitations, for example, when a material is driven out of equilibrium by a short laser pulse. In a pioneering experiment, time-resolved RIXS was used to study how magnetic correlation evolves upon photodoping the Sr_2IrO_4 Mott insulator[147]. The 3D magnetic order, measured by time-resolved resonant elastic soft X-ray scattering, was completely quenched within the first 2 ps and recovered with a fluence-dependent time constant that varied between 100 ps and 1 ns. Time-resolved RIXS was then used to examine the evolution of magnetic excitations and revealed that 2D in-plane magnetic correlations recover on a much faster timescale than the 3D magnetic order. It was speculated that such a fast recovery time, which is similar to that of charge recombination, might be due to the fundamental link that exists in strongly correlated materials between the in-plane electron hopping parameter and the in-plane magnetic exchange. The slow recovery of the long-range magnetic order was instead related to the weak inter-plane exchange coupling and energy dissipation into other degrees of freedom.

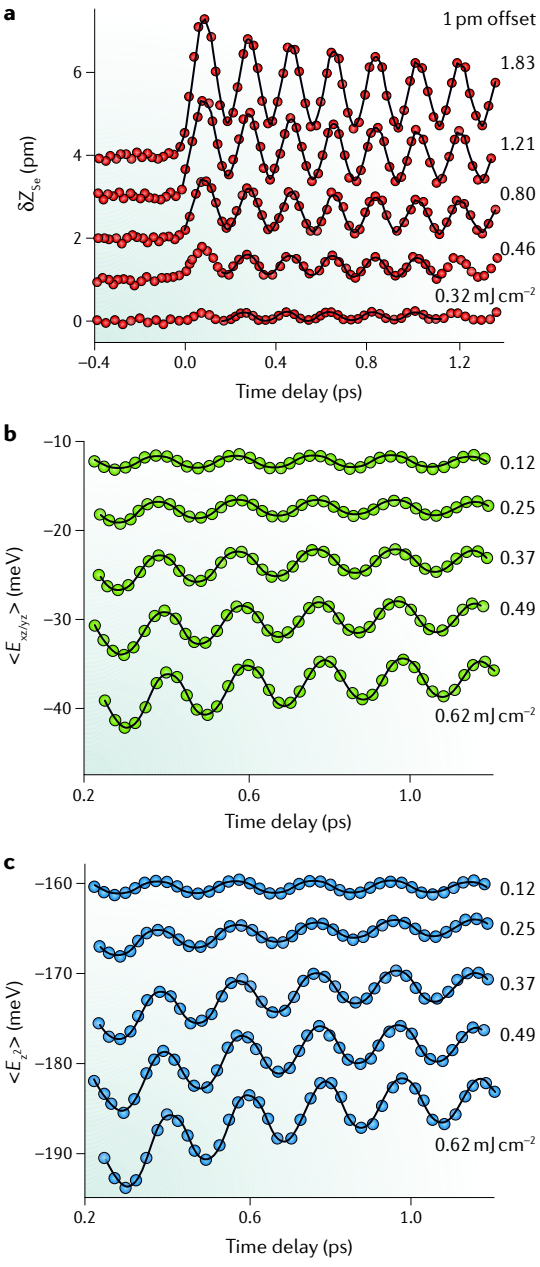

Fig. 5 | **Electron–phonon deformation potential in an iron-based superconductor.** The orbital-resolved electron–phonon deformation potential in an FeSe superconducting thin film was determined using time-resolved X-ray diffraction and time-resolved and angular-resolved photoemission spectroscopy (tr-ARPES). **a** | Displacement of the Se atom, δZ_{Se}, extracted from the evolution of the intensity of the (004) Bragg peak. **b**,**c** | Momentum-averaged energy shifts $<E>$ of the $d_{XZ/YZ}$ and d_{Z^2} bands extracted from tr-ARPES measurements. All measurements are shown for different photoexcitation levels, ranging from 0.12 to 1.83 mJ cm^{-2}. Adapted with permission from REF.[139], AAAS.

Fourier-transform inelastic X-ray scattering. Short X-ray pulses also allow for inelastic measurements of non-equilibrium lattice dynamics. In 2013, a new and highly interesting experimental technique to probe phonon dispersion curves in solids by measuring time-resolved X-ray scattering[148] was demonstrated. In this experiment, a single crystal of Ge was excited with near-infrared laser pulses to produce correlated phonon pairs with equal and opposite momenta that modulate the X-ray diffuse scattering intensity around Bragg peaks at twice the phonon frequency. In contrast to typical X-ray measurements that analyse the incoherent thermal diffuse scattering and require an ab initio model of the interatomic forces, this method enables the phonon dispersion curves to be extracted directly from Fourier transformations of the modulated diffuse scattering intensity. The dispersion relations of two transverse acoustic modes in Ge, measured along the directions illustrated in FIG. 6a, are shown in FIG. 6b,c. The agreement with the calculated dispersions (white lines) is good, especially considering that there are no adjustable parameters. Fourier-transform inelastic X-ray scattering was also used to investigate the origin of incipient ferroelectricity in PbTe. The ferroelectric instability was found to be due to the existence of strong electron–phonon interactions rather than phonon–phonon anharmonicities[149].

Probing excitations in the time domain also has significant advantages over equilibrium measurements such as inelastic neutron and X-ray scattering. For example, Fourier-transform inelastic X-ray scattering in the time domain allows for easier access to the lower-frequency part of the dispersion relations of an excitation. Furthermore, traditional inelastic measurements reveal only harmonic properties of phonons in a momentum-resolved manner, whereas time-resolved X-ray scattering can reveal the presence of anharmonic coupling between different phonon modes. In a recent experiment, the individual decay channel of the A_{1g} phonon mode in Bi was directly identified[150]. In this experiment, anharmonic force constants between the A_{1g} mode and the anharmonically coupled longitudinal acoustic modes were quantitatively measured for the first time.

Conclusions and future perspectives

All the experiments discussed above demonstrate how the advent of short X-ray pulses has enabled a far deeper understanding of non-equilibrium phenomena in complex solids. In most cases, FEL operation is based on self-amplified spontaneous emission, which produces pulses with a large bandwidth and strong shot-to-shot fluctuations in most of the key parameters, such as intensity, duration and spectrum[40]. Although these fluctuations can often be accounted for using single-shot diagnostics[151–153], the large bandwidth of the X-ray pulses severely limits the energy resolution achieved during experiments. This problem is typically mitigated by the use of monochromators, with the caveat that they cause a severe reduction (up to two orders of magnitude) in the available X-ray intensity.

To overcome the limitations in energy resolution and stability of the source, a key aspect in the design of advanced FEL sources is the adoption of seeding schemes with the ultimate aim of reaching Fourier-transform-limited X-ray pulses[154–156]. Compared with self-amplified spontaneous emission operation, seeded FEL operation produces pulses with a narrower

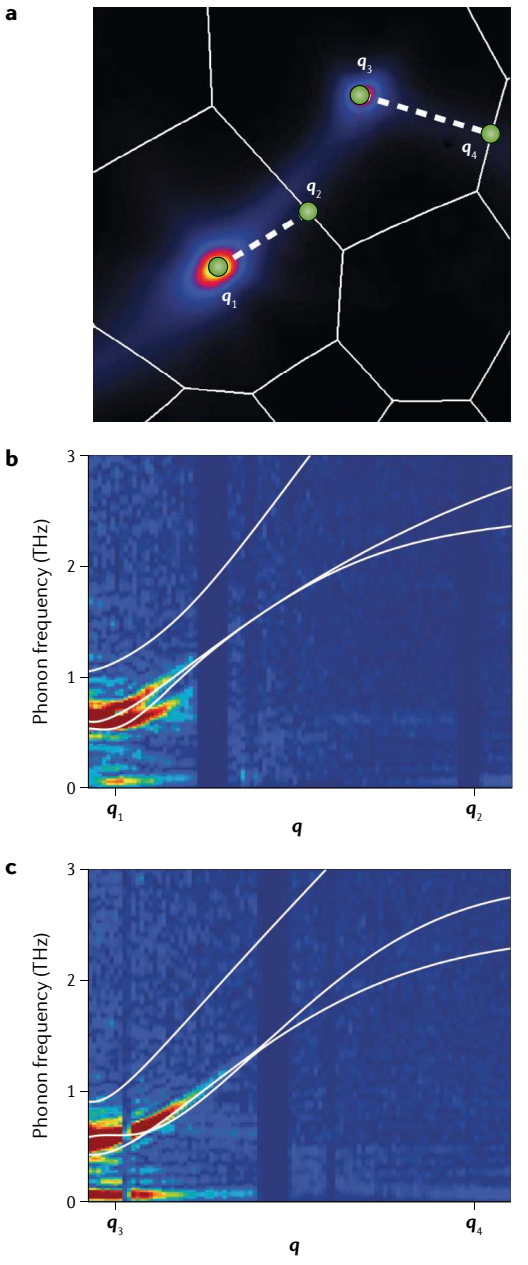

Fig. 6 | **Phonon dispersion relation in germanium.** The dispersion relations of the two transverse acoustic branches of Ge were obtained using Fourier-transform inelastic X-ray scattering. The calculated equilibrium diffraction pattern is shown in panel **a**; the dashed lines indicate the directions along which the dispersion relations are shown in panel **b** as a function of the reciprocal space vector $\boldsymbol{q}$, where $\boldsymbol{q}_1 = (-0.1, 0, -0.07)$ and $\boldsymbol{q}_2 = (-0.33, -0.75, 0.37)$, and in panel **c**, where $\boldsymbol{q}_3 = (0.13, -0.04, 0.05)$ and $\boldsymbol{q}_4 = (-0.09, -0.98, -0.08)$ (reciprocal lattice units). The solid white lines in panels **b** and **c** represent the calculated acoustic dispersion curves. Adapted from REF.[148], Macmillan Publishers Limited.

bandwidth and significantly improved energy and intensity stability. Another important benefit of newly developed FEL sources is the increase in pulse repetition rate, which enables faster data collection. In combination, we expect that seeded FEL sources with high repetition rates will foster a number of 'flux-hungry' techniques, such as time-resolved resonant X-ray diffraction or RIXS, with even higher time and spectral resolution.

Finally, these new sources promise complete control of the X-ray pulse parameters and may enable us to achieve the aim of obtaining pulses with sub-femtosecond durations and arbitrary pulse shapes. With more precise synchronization between the X-ray pulses and the optical excitation fields, as in the case of terahertz and mid-infrared pulses[157], it is already becoming possible to stabilize X-ray pulses with respect to the absolute phase of the pump pulses. We envision that this advancement will open up entirely new areas of research in the investigation of coherence effects. For example, it will be possible to follow changes in material structure and electronic properties as they are induced by the excitation electric field, promising further insight into the origin of nonlinear couplings between different excitations in condensed matter.

Published online 1 June 2018

1. Devereaux, T. P. & Hackl, R. Inelastic light scattering from correlated electrons. *Rev. Mod. Phys.* **79**, 175–233 (2007).
2. Fink, J., Schierle, E., Weschke, E. & Geck, J. Resonant elastic soft x-ray scattering. *Rep. Prog. Phys.* **76**, 056502 (2013).
3. Damascelli, A. Probing the electronic structure of complex systems by ARPES. *Phys. Scr.* **2004**, 61 (2004).
4. Damascelli, A., Hussain, Z. & Shen, Z.-X. Angle-resolved photoemission studies of the cuprate superconductors. *Rev. Mod. Phys.* **75**, 473–541 (2003).
5. Graves, C. E. et al. Nanoscale spin reversal by non-local angular momentum transfer following ultrafast laser excitation in ferrimagnetic GdFeCo. *Nat. Mater.* **12**, 293–298 (2013).
6. Stanciu, C. D. et al. All-optical magnetic recording with circularly polarized light. *Phys. Rev. Lett.* **99**, 047601 (2007).
7. Mankowsky, R., von Hoegen, A., Först, M. & Cavalleri, A. Ultrafast reversal of the ferroelectric polarization. *Phys. Rev. Lett.* **118**, 197601 (2017).
8. Chen, F. et al. Ultrafast terahertz-field-driven ionic response in ferroelectric $BaTiO_3$. *Phys. Rev. B* **94**, 180104 (2016).
9. de Jong, S. et al. Speed limit of the insulator–metal transition in magnetite. *Nat. Mater.* **12**, 882–886 (2013).
10. Rini, M. et al. Control of the electronic phase of a manganite by mode-selective vibrational excitation. *Nature* **449**, 72–74 (2007).
11. Fausti, D. et al. Light-induced superconductivity in a stripe-ordered cuprate. *Science* **331**, 189–191 (2011).
12. Hu, W. et al. Optically enhanced coherent transport in $YBa_2Cu_3O_{6.5}$ by ultrafast redistribution of interlayer coupling. *Nat. Mater.* **13**, 705–711 (2014).
13. Mitrano, M. et al. Possible light-induced superconductivity in K_3C_{60} at high temperature. *Nature* **530**, 461–464 (2016).
14. Wang, X. et al. Measurement of femtosecond electron pulse length and the temporal broadening due to space charge. *Rev. Sci. Instrum.* **80**, 013902 (2009).
15. Shank, C. V. & Ippen, E. P. Subpicosecond kilowatt pulses from a mode-locked cw dye laser. *Appl. Phys. Lett.* **24**, 373–375 (1974).
16. Fork, R. L., Greene, B. I. & Shank, C. V. Generation of optical pulses shorter than 0.1 psec by colliding pulse mode locking. *Appl. Phys. Lett.* **38**, 671–672 (1981).
17. Strickland, D. & Mourou, G. Compression of amplified chirped optical pulses. *Opt. Commun.* **56**, 219–221 (1985).
18. Knox, W. H. Femtosecond optical pulse amplification. *IEEE J. Quantum Electron.* **24**, 388–397 (1988).
19. Murnane, M. M., Kapteyn, H. C., Rosen, M. D. & Falcone, R. W. Ultrafast X-ray pulses from laser-produced plasmas. *Science* **251**, 531–536 (1991).
20. Rousse, A. et al. Efficient *K* α x-ray source from femtosecond laser-produced plasmas. *Phys. Rev. E* **50**, 2200–2207 (1994).
21. Rischel, C. et al. Femtosecond time-resolved X-ray diffraction from laser-heated organic films. *Nature* **390**, 490–492 (1997).
22. Siders, C. W. et al. Detection of nonthermal melting by ultrafast X-ray diffraction. *Science* **286**, 1340–1342 (1999).
23. Sokolowski-Tinten, K. et al. Femtosecond X-ray measurement of ultrafast melting and large acoustic transients. *Phys. Rev. Lett.* **87**, 225701 (2001).
24. Rousse, A. et al. Non-thermal melting in semiconductors measured at femtosecond resolution. *Nature* **410**, 65–68 (2001).
25. Rose-Petruck, C. et al. Picosecond-milliångstrom lattice dynamics measured by ultrafast X-ray diffraction. *Nature* **398**, 310–312 (1999).
26. Cavalleri, A. et al. Anharmonic lattice dynamics in germanium measured with ultrafast X-ray diffraction. *Phys. Rev. Lett.* **85**, 586–589 (2000).
27. Sokolowski-Tinten, K. et al. Femtosecond X-ray measurement of coherent lattice vibrations near the Lindemann stability limit. *Nature* **422**, 287–289 (2003).
28. Cavalleri, A. et al. Femtosecond structural dynamics in VO_2 during an ultrafast solid-solid phase transition. *Phys. Rev. Lett.* **87**, 237401 (2001).
29. Schoenlein, R. W. et al. Femtosecond X-ray pulses at 0.4 Å generated by 90° Thomson scattering: a tool for probing the structural dynamics of materials. *Science* **274**, 236–238 (1996).
30. Leemans, W. P. et al. X-ray based subpicosecond electron bunch characterization using 90° Thomson scattering. *Phys. Rev. Lett.* **77**, 4182–4185 (1996).
31. Chin, A. H. et al. Ultrafast structural dynamics in InSb probed by time-resolved X-ray diffraction. *Phys. Rev. Lett.* **83**, 336–339 (1999).
32. Zholents, A. A. & Zolotorev, M. S. Femtosecond X-ray pulses of synchrotron radiation. *Phys. Rev. Lett.* **76**, 912–915 (1996).
33. Schoenlein, R. W. et al. Generation of femtosecond pulses of synchrotron radiation. *Science* **287**, 2237–2240 (2000).
34. Cavalleri, A. et al. Tracking the motion of charges in a terahertz light field by femtosecond X-ray diffraction. *Nature* **442**, 664–666 (2006).
35. Johnson, S. L. et al. Nanoscale depth-resolved coherent femtosecond motion in laser-excited bismuth. *Phys. Rev. Lett.* **100**, 155501 (2008).
36. Cavalleri, A. et al. Band-selective measurements of electron dynamics in VO_2 using femtosecond near-edge X-ray absorption. *Phys. Rev. Lett.* **95**, 067405 (2005).
37. Stamm, C. et al. Femtosecond modification of electron localization and transfer of angular momentum in nickel. *Nat. Mater.* **6**, 740–743 (2007).
38. Gaffney, K. J. et al. Observation of structural anisotropy and the onset of liquidlike motion during the nonthermal melting of InSb. *Phys. Rev. Lett.* **95**, 125701 (2005).
39. Fritz, D. M. et al. Ultrafast bond softening in bismuth: mapping a solid's interatomic potential with X-rays. *Science* **315**, 633–636 (2007).
40. Emma, P. et al. First lasing and operation of an ångstrom-wavelength free-electron laser. *Nat. Photonics* **4**, 641–647 (2010).
41. Landauer, R. Electrostatic considerations in $BaTiO_3$ domain formation during polarization reversal. *J. Appl. Phys.* **28**, 227–234 (1957).
42. Li, J. et al. Ultrafast polarization switching in thin-film ferroelectrics. *Appl. Phys. Lett.* **84**, 1174–1176 (2004).
43. Kenjiro, F. & Yasuo, C. Nanosecond switching of nanoscale ferroelectric domains in congruent single-crystal $LiTaO_3$ using scanning nonlinear dielectric microscopy. *Jpn J. Appl. Phys.* **43**, 2818 (2004).
44. Fahy, S. & Merlin, R. Reversal of ferroelectric domains by ultrashort optical pulses. *Phys. Rev. Lett.* **73**, 1122–1125 (1994).
45. Brennan, C. J. & Nelson, K. A. Direct time-resolved measurement of anharmonic lattice vibrations in ferroelectric crystals. *J. Chem. Phys.* **107**, 9691–9694 (1997).
46. Istomin, K., Kotaidis, V., Plech, A. & Kong, Q. Y. Dynamics of the laser-induced ferroelectric excitation in $BaTiO_3$ studied by X-ray diffraction. *Appl. Phys. Lett.* **90**, 022905 (2007).
47. Qi, T., Shin, Y. H., Yeh, K. L., Nelson, K. A. & Rappe, A. M. Collective coherent control: synchronization of polarization in ferroelectric $PbTiO_3$ by shaped THz fields. *Phys. Rev. Lett.* **102**, 247603 (2009).
48. Liu, H. D. et al. In situ observation of light-assisted domain reversal in lithium niobate crystals. *Opt. Mater. Express* **1**, 1433–1438 (2011).
49. Zhi, Y. N., Liu, D. A., Qu, W. J., Luan, Z. & Liu, L. R. Wavelength dependence of light-induced domain nucleation in MgO-doped congruent $LiNbO_3$ crystal. *Appl. Phys. Lett.* **90**, 042904 (2007).
50. Ying, C. Y. et al. Ultra-smooth lithium niobate photonic micro-structures by surface tension reshaping. *Opt. Express* **18**, 11508–11513 (2010).
51. Steigerwald, H., von Cube, F., Luedtke, F., Dierolf, V. & Buse, K. Influence of heat and UV light on the coercive field of lithium niobate crystals. *Appl. Phys. B* **101**, 535–539 (2010).
52. Daranciang, D. et al. Ultrafast photovoltaic response in ferroelectric nanolayers. *Phys. Rev. Lett.* **108**, 087601 (2012).
53. Lichtensteiger, C. et al. in *Oxide Ultrathin Films* (eds Pacchioni, G. & Valeri, S.) 265–230 (Wiley-VCH, Weinheim, Germany, 2011).
54. Grübel, S. et al. Ultrafast x-ray diffraction of a ferroelectric soft mode driven by broadband terahertz pulses. Preprint at *arXiv*, 1602.05435 (2016).
55. Subedi, A. Midinfrared-light-induced ferroelectricity in oxide paraelectrics via nonlinear phononics. *Phys. Rev. B* **95**, 134113 (2017).
56. Pitaevskii, L. P. Electric forces in a transparent dispersive medium. *J. Exp. Theor. Phys.* **12**, 1008–1013 (1961).
57. Pershan, P. S., van der Ziel, J. P. & Malmstrom, L. D. Theoretical discussion of the inverse Faraday effect, Raman scattering, and related phenomena. *Phys. Rev.* **143**, 574–583 (1966).
58. van der Ziel, J. P., Pershan, P. S. & Malmstrom, L. D. Optically-induced magnetization resulting from the inverse Faraday effect. *Phys. Rev. Lett.* **15**, 190–193 (1965).
59. Beaurepaire, E., Merle, J., Daunois, A. & Bigot, J. Ultrafast spin dynamics in ferromagnetic nickel. *Phys. Rev. Lett.* **76**, 4250–4253 (1996).
60. Mangin, S. et al. Engineered materials for all-optical helicity-dependent magnetic switching. *Nat. Mater.* **13**, 286–292 (2014).
61. Lambert, C. H. et al. All-optical control of ferromagnetic thin films and nanostructures. *Science* **345**, 1337–1340 (2014).
62. Battiato, M., Carva, K. & Oppeneer, P. M. Superdiffusive spin transport as a mechanism of ultrafast demagnetization. *Phys. Rev. Lett.* **105**, 027203 (2010).
63. Gutt, C. et al. Single-pulse resonant magnetic scattering using a soft x-ray free-electron laser. *Phys. Rev. B* **81**, 100401 (2010).
64. Pfau, B. et al. Ultrafast optical demagnetization manipulates nanoscale spin structure in domain walls. *Nat. Commun.* **3**, 1100 (2012).
65. Stavrou, E., Sbiaa, R., Suzuki, T., Knappmann, S. & Röll, K. Magnetic anisotropy and spin reorientation effects in Gd/Fe and Gd/(FeCo) multilayers for high

density magneto-optical recording. *J. Appl. Phys.* **87**, 6899–6901 (2000).
66. Ostler, T. A. et al. Ultrafast heating as a sufficient stimulus for magnetization reversal in a ferrimagnet. *Nat. Commun.* **3**, 666 (2012).
67. Le Guyader, L. et al. Nanoscale sub-100 picosecond all-optical magnetization switching in GdFeCo microstructures. *Nat. Commun.* **6**, 5839 (2015).
68. Staub, U. Advanced resonant soft x-ray diffraction to study ordering phenomena in magnetic materials. *J. Phys. Conf. Ser.* **211**, 012003 (2010).
69. Comin, R. & Damascelli, A. Resonant X-ray scattering studies of charge order in cuprates. *Annu. Rev. Condens. Matter Phys.* **7**, 369–405 (2016).
70. Holldack, K. et al. Ultrafast dynamics of antiferromagnetic order studied by femtosecond resonant soft x-ray diffraction. *Appl. Phys. Lett.* **97**, 062502 (2010).
71. Rettig, L. et al. Itinerant and localized magnetization dynamics in antiferromagnetic Ho. *Phys. Rev. Lett.* **116**, 257202 (2016).
72. Eisebitt, S. et al. Lensless imaging of magnetic nanostructures by X-ray spectro-holography. *Nature* **432**, 885–888 (2004).
73. Wang, T. et al. Femtosecond single-shot imaging of nanoscale ferromagnetic order in Co/Pd multilayers using resonant x-ray holography. *Phys. Rev. Lett.* **108**, 267403 (2012).
74. von Korff Schmising, C. et al. Imaging ultrafast demagnetization dynamics after a spatially localized optical excitation. *Phys. Rev. Lett.* **112**, 217203 (2014).
75. Seaberg, M. H. et al. Nanosecond X-ray photon correlation spectroscopy on magnetic skyrmions. *Phys. Rev. Lett.* **119**, 067403 (2017).
76. Verwey, E. J. W. Electronic conduction of magnetite (Fe_3O_4) and its transition point at low temperatures. *Nature* **144**, 327–328 (1939).
77. Senn, M. S., Wright, J. P. & Attfield, J. P. Charge order and three-site distortions in the Verwey structure of magnetite. *Nature* **481**, 173–176 (2012).
78. Zimmermann, M.v. et al. Interplay between charge, orbital, and magnetic order in $Pr_{1-x}Ca_xMnO_3$. *Phys. Rev. Lett.* **83**, 4872–4875 (1999).
79. Staub, U. et al. Direct observation of charge order in an epitaxial $NdNiO_3$ film. *Phys. Rev. Lett.* **88**, 126402 (2002).
80. Beaud, P. et al. A time-dependent order parameter for ultrafast photoinduced phase transitions. *Nat. Mater.* **13**, 923–927 (2014).
81. Tokura, Y. & Nagaosa, N. Orbital physics in transition-metal oxides. *Science* **288**, 462–468 (2000).
82. Esposito, V. et al. Nonlinear electron-phonon coupling in doped manganites. *Phys. Rev. Lett.* **118**, 247601 (2017).
83. Sternlieb, B. J. et al. Charge and magnetic order in $La_{0.5}Sr_{1.5}MnO_4$. *Phys. Rev. Lett.* **76**, 2169–2172 (1996).
84. Tobey, R. I. et al. Evolution of three-dimensional correlations during the photoinduced melting of antiferromagnetic order in $La_{0.5}Sr_{1.5}MnO_4$. *Phys. Rev. B* **86**, 064425 (2012).
85. Ehrke, H. et al. Photoinduced melting of antiferromagnetic order in $La_{0.5}Sr_{1.5}MnO_4$ measured using ultrafast resonant soft x-ray diffraction. *Phys. Rev. Lett.* **106**, 217401 (2011).
86. Först, M. et al. Driving magnetic order in a manganite by ultrafast lattice excitation. *Phys. Rev. B* **84**, 241104 (2011).
87. Först, M. et al. Nonlinear phononics as an ultrafast route to lattice control. *Nat. Phys.* **7**, 854–856 (2011).
88. Först, M. et al. Displacive lattice excitation through nonlinear phononics viewed by femtosecond X-ray diffraction. *Solid State Commun.* **169**, 24–27 (2013).
89. Mankowsky, R., Först, M. & Cavalleri, A. Non-equilibrium control of complex solids by nonlinear phononics. *Rep. Prog. Phys.* **79**, 064503 (2016).
90. Yoshizawa, H. et al. Stripe order at low temperatures in $La_{2-x}Sr_xNiO_4$ with $0.289 \lesssim x \lesssim 0.5$. *Phys. Rev. B* **61**, R854–R857 (2000).
91. Schussler-Langeheine, C. et al. Spectroscopy of stripe order in $La_{1.8}Sr_{0.2}NiO_4$ using resonant soft x-ray diffraction. *Phys. Rev. Lett.* **95**, 156402 (2005).
92. Lee, W. S. et al. Phase fluctuations and the absence of topological defects in a photo-excited charge-ordered nickelate. *Nat. Commun.* **3**, 838 (2012).
93. Chuang, Y. D. et al. Real-time manifestation of strongly coupled spin and charge order parameters in stripe-ordered $La_{1.75}Sr_{0.25}NiO_4$ nickelate crystals using time-resolved resonant x-ray diffraction. *Phys. Rev. Lett.* **110**, 127404 (2013).
94. Lee, W. S. et al. Nonequilibrium lattice-driven dynamics of stripes in nickelates using time-resolved x-ray scattering. *Phys. Rev. B* **95**, 121105 (2017).
95. Fiebig, M. Revival of the magnetoelectric effect. *J. Phys. D* **38**, R123–R152 (2005).
96. Eerenstein, W., Mathur, N. D. & Scott, J. F. Multiferroic and magnetoelectric materials. *Nature* **442**, 759–765 (2006).
97. Spaldin, N. A. Multiferroics: past, present, and future. *MRS Bull.* **42**, 385–390 (2017).
98. Kubacka, T. et al. Large-amplitude spin dynamics driven by a THz pulse in resonance with an electromagnon. *Science* **343**, 1333–1336 (2014).
99. Johnson, S. L. et al. Femtosecond dynamics of the collinear-to-spiral antiferromagnetic phase transition in CuO. *Phys. Rev. Lett.* **108**, 037203 (2012).
100. Yang, B. X., Thurston, T. R., Tranquada, J. M. & Shirane, G. Magnetic neutron scattering study of single-crystal cupric oxide. *Phys. Rev. B* **39**, 4343–4349 (1989).
101. Langner, M. C. et al. Nonlinear ultrafast spin scattering in the skyrmion phase of Cu_2OSeO_3. *Phys. Rev. Lett.* **119**, 107204 (2017).
102. Okamura, Y., Kagawa, F., Seki, S. & Tokura, Y. Transition to and from the skyrmion lattice phase by electric fields in a magnetoelectric compound. *Nat. Commun.* **7**, 12669 (2016).
103. Mühlbauer, S. et al. Skyrmion lattice in a chiral magnet. *Science* **323**, 915–919 (2009).
104. Hwang, H. Y. et al. Emergent phenomena at oxide interfaces. *Nat. Mater.* **11**, 103–113 (2012).
105. Caviglia, A. D. et al. Ultrafast strain engineering in complex oxide heterostructures. *Phys. Rev. Lett.* **108**, 136801 (2012).
106. Först, M. et al. Spatially resolved ultrafast magnetic dynamics initiated at a complex oxide heterointerface. *Nat. Mater.* **14**, 883–888 (2015).
107. Först, M. et al. Multiple supersonic phase fronts launched at a complex-oxide heterointerface. *Phys. Rev. Lett.* **118**, 027401 (2017).
108. Grüner, G. *Density Waves in Solids.* (Addison-Wesley, Reading, MA, 1994).
109. Peierls, R. E. *Quantum Theory of Solids.* (Oxford Univ. Press, Oxford, UK, 1955).
110. Perfetti, L. et al. Time evolution of the electronic structure of 1*T*-TaS_2 through the insulator-metal transition. *Phys. Rev. Lett.* **97**, 067402 (2006).
111. Dean, N. et al. Polaronic conductivity in the photoinduced phase of 1*T*-TaS_2. *Phys. Rev. Lett.* **106**, 016401 (2011).
112. Petersen, J. C. et al. Clocking the melting transition of charge and lattice order in 1*T*-TaS_2 with ultrafast extreme-ultraviolet angle-resolved photoemission spectroscopy. *Phys. Rev. Lett.* **107**, 177402 (2011).
113. Eichberger, M. et al. Snapshots of cooperative atomic motions in the optical suppression of charge density waves. *Nature* **468**, 799–802 (2010).
114. Stojchevska, L. et al. Ultrafast switching to a stable hidden quantum state in an electronic crystal. *Science* **344**, 177–180 (2014).
115. Schäfer, H., Kabanov, V. V. & Demsar, J. Collective modes in quasi-one-dimensional charge-density wave systems probed by femtosecond time-resolved optical studies. *Phys. Rev. B* **89**, 045106 (2014).
116. Schäfer, H., Kabanov, V. V., Beyer, M., Biljakovic, K. & Demsar, J. Disentanglement of the electronic and lattice parts of the order parameter in a 1D charge density wave system probed by femtosecond spectroscopy. *Phys. Rev. Lett.* **105**, 066402 (2010).
117. Liu, H. Y. et al. Possible observation of parametrically amplified coherent phasons in $K_{0.3}MoO_3$ using time-resolved extreme-ultraviolet angle-resolved photoemission spectroscopy. *Phys. Rev. B* **88**, 045104 (2013).
118. Tomeljak, A. et al. Dynamics of photoinduced charge-density-wave to metal phase transition in $K_{0.3}MoO_3$. *Phys. Rev. Lett.* **102**, 066404 (2009).
119. Huber, T. et al. Coherent structural dynamics of a prototypical charge-density-wave-to-metal transition. *Phys. Rev. Lett.* **113**, 026401 (2014).
120. Mankowsky, R. et al. Dynamical stability limit for the charge density wave in $K_{0.3}MoO_3$. *Phys. Rev. Lett.* **118**, 116402 (2017).
121. Huber, J. G., Liverman, W. J., Xu, Y. & Moodenbaugh, A. R. Superconductivity under high pressure of $YBa_2(Cu_{1-x}Mx)_3O_{7-\delta}$ M = Fe, Co, Al, Cr, Ni, and Zn. *Phys. Rev. B* **41**, 8757–8761 (1990).
122. Schirber, J. E., Ginley, D. S., Venturini, E. L. & Morosin, B. Pressure dependence of the superconducting transition temperature in the 94-K superconductor $YBa_2Cu_3O_7$. *Phys. Rev. B* **35**, 8709–8710 (1987).
123. Bucher, B., Karpinski, J., Kaldis, E. & Wachter, P. Pressure dependence of T_c and anisotropic features in the family $Y_2Ba_4Cu_{6+n}O_{14+n}$ (n = 0,1,2). *J. Less-Common Met.* **164**, 20–30 (1990).
124. Cyr-Choinière, O. et al. Suppression of charge order by pressure in the cuprate superconductor YBa_2Cu_3Oy: restoring the full superconducting dome. Preprint at *arXiv*, 1503.02033 (2015).
125. Kaiser, S. et al. Optically induced coherent transport far above T_c in underdoped $YBa_2Cu_3O_{6+\delta}$. *Phys. Rev. B* **89**, 184516 (2014).
126. Mankowsky, R. et al. Nonlinear lattice dynamics as a basis for enhanced superconductivity in $YBa_2Cu_3O_{6.5}$. *Nature* **516**, 71–73 (2014).
127. Mankowsky, R. et al. Optically induced lattice deformations, electronic structure changes, and enhanced superconductivity in $YBa_2Cu_3O_{6.48}$. *Struct. Dyn.* **4**, 044007 (2017).
128. Ghiringhelli, G. et al. Long-range incommensurate charge fluctuations in $(Y,Nd)Ba_2Cu_3O_{(6+x)}$. *Science* **337**, 821–825 (2012).
129. Chang, J. et al. Direct observation of competition between superconductivity and charge density wave order in $YBa_2Cu_3O_{6.67}$. *Nat. Phys.* **8**, 871–876 (2012).
130. Tranquada, J. M., Sternlieb, B. J., Axe, J. D., Nakamura, Y. & Uchida, S. Evidence for stripe correlations of spins and holes in copper oxide superconductors. *Nature* **375**, 561–563 (1995).
131. Hücker, M. et al. Stripe order in superconducting $La_{2-x}Ba_xCuO_4$ ($0.095 \le x \le 0.155$). *Phys. Rev. B* **83**, 104506 (2011).
132. Först, M. et al. Melting of charge stripes in vibrationally driven $La_{1.875}Ba_{0.125}CuO_4$: assessing the respective roles of electronic and lattice order in frustrated superconductors. *Phys. Rev. Lett.* **112**, 157002 (2014).
133. Khanna, V. et al. Restoring interlayer Josephson coupling in $La_{1.885}Ba_{0.115}CuO_4$ by charge transfer melting of stripe order. *Phys. Rev. B* **93**, 224522 (2016).
134. Först, M. et al. Femtosecond x rays link melting of charge-density wave correlations and light-enhanced coherent transport in $YBa_2Cu_3O_{6.6}$. *Phys. Rev. B* **90**, 184514 (2014).
135. Yang, L. X. et al. Ultrafast modulation of the chemical potential in $BaFe_2As_2$ by coherent phonons. *Phys. Rev. Lett.* **112**, 207001 (2014).
136. Gerber, S. et al. Direct characterization of photoinduced lattice dynamics in $BaFe_2As_2$. *Nat. Commun.* **6**, 7377 (2015).
137. Rettig, L. et al. Ultrafast structural dynamics of the Fe-pnictide parent compound $BaFe_2As_2$. *Phys. Rev. Lett.* **114**, 067402 (2015).
138. Mandal, S., Cohen, R. E. & Haule, K. Strong pressure-dependent electron-phonon coupling in FeSe. *Phys. Rev. B* **89**, 220502 (2014).
139. Gerber, S. et al. Femtosecond electron-phonon lock-in by photoemission and x-ray free-electron laser. *Science* **357**, 71–75 (2017).
140. Ament, L. J. P., van Veenendaal, M., Devereaux, T. P., Hill, J. P. & van den Brink, J. Resonant inelastic x-ray scattering studies of elementary excitations. *Rev. Mod. Phys.* **83**, 705–767 (2011).
141. Ghiringhelli, G. et al. NiO as a test case for high resolution resonant inelastic soft x-ray scattering. *J. Phys. Condens. Matter* **17**, 5397–5412 (2005).
142. Ishii, H. et al. Resonant soft X-ray emission spectroscopy of NiO across the Ni $L_{2,3}$ thresholds. *J. Phys. Soc. Jpn* **70**, 1813–1816 (2001).
143. Ishii, K. et al. Momentum-resolved electronic excitations in the Mott insulator Sr_2IrO_4 studied by resonant inelastic x-ray scattering. *Phys. Rev. B* **83**, 115121 (2011).
144. Ghiringhelli, G. et al. Observation of two nondispersive magnetic excitations in NiO by resonant inelastic soft-X-ray scattering. *Phys. Rev. Lett.* **102**, 027401 (2009).
145. Yavas, H. et al. Observation of phonons with resonant inelastic x-ray scattering. *J. Phys. Condens. Matter* **22**, 485601 (2010).
146. Braicovich, L. et al. Magnetic excitations and phase separation in the underdoped $La_{2-x}Sr_xCuO_4$ superconductor measured by resonant inelastic X-ray scattering. *Phys. Rev. Lett.* **104**, 077002 (2010).
147. Dean, M. P. M. et al. Ultrafast energy- and momentum-resolved dynamics of magnetic correlations in the photo-doped Mott insulator Sr_2IrO_4. *Nat. Mater.* **15**, 601–605 (2016).
148. Trigo, M. et al. Fourier-transform inelastic X-ray scattering from time- and momentum-dependent phonon-phonon correlations. *Nat. Phys.* **9**, 790–794 (2013).

149. Jiang, M. P. et al. The origin of incipient ferroelectricity in lead telluride. *Nat. Commun.* **7**, 12291 (2016).
150. Teitelbaum, S. W. et al. Direct measurement of anharmonic decay channels of a coherent phonon. *Preprint at arXiv* **1710**, 02207 (2017).
151. Harmand, M. et al. Achieving few-femtosecond time-sorting at hard X-ray free-electron lasers. *Nat. Photonics* **7**, 215–218 (2013).
152. Zhu, D. et al. A single-shot transmissive spectrometer for hard x-ray free electron lasers. *Appl. Phys. Lett.* **101**, 034103 (2012).
153. Hartmann, N. et al. Sub-femtosecond precision measurement of relative X-ray arrival time for free-electron lasers. *Nat. Photonics* **8**, 706–709 (2014).
154. Allaria, E. et al. Highly coherent and stable pulses from the FERMI seeded free-electron laser in the extreme ultraviolet. *Nat. Photonics* **6**, 699–704 (2012).
155. Amann, J. et al. Demonstration of self-seeding in a hard-X-ray free-electron laser. *Nat. Photonics* **6**, 693–698 (2012).
156. Ratner, D. et al. Experimental demonstration of a soft X-ray self-seeded free-electron laser. *Phys. Rev. Lett.* **114**, 054801 (2015).
157. Grguraš, I. et al. Ultrafast X-ray pulse characterization at free-electron lasers. *Nat. Photonics* **6**, 852–857 (2012).
158. Bressler, C. et al. Femtosecond XANES study of the light-induced spin crossover dynamics in an iron(II) complex. *Science* **323**, 489–492 (2009).
159. Radu, I. et al. Transient ferromagnetic-like state mediating ultrafast reversal of antiferromagnetically coupled spins. *Nature* **472**, 205–208 (2011).

Acknowledgements
The authors acknowledge funding from the European Research Council (ERC) under the European Union's Seventh Framework Programme (FP7/2007-2013)/ERC Grant No. 319286 (Q-MAC) and acknowledge support from the Deutsche Forschungsgemeinschaft through the Hamburg Centre for Ultrafast Imaging — Structure, Dynamics and Control of Matter at the Atomic Scale excellence cluster and the priority programme SFB925. M.B. acknowledges financial support from the Swiss National Science Foundation through an Early Postdoc Mobility Grant (P2BSP2_165352).

Author contributions
All authors contributed equally to the preparation of this article.

Competing interests
The authors declare no competing interests.

Publisher's note
Springer Nature remains neutral with regard to jurisdictional claims in published maps and institutional affiliations.